Available online at www.sciencedirect.com
SCIENCE DIRECT®
International Journal of Solids and Structures 43 (2006) 5501–5524
INTERNATIONAL JOURNAL OF SOLIDS and STRUCTURES
www.elsevier.com/locate/ijsolstr

Postcritical imperfection sensitivity of sandwich or homogenized orthotropic columns soft in shear and in transverse deformation

Alessandro Beghini [a], Zdeněk P. Bažant [b,*], Anthony M. Waas [c], Shiladitya Basu [c]

[a] *Skidmore, Owings & Merrill LLP, Chicago, IL 60604, USA*
[b] *Department of Civil and Environmental Engineering, Northwestern University, Evanston, IL 60208, USA*
[c] *Department of Aerospace Engineering, University of Michigan, Ann Arbor, MI 48109, USA*

Received 30 April 2005; received in revised form 8 July 2005
Available online 23 September 2005

Abstract

The previous energetic variational analysis of critical loads and of the choice of finite strain measure for structures very weak in shear, remaining in a state of small strain, is extended to the initial postcritical behavior. For this purpose, consideration of the transverse deformation is found to be essential. It is shown that imperfection sensitivity of such structures, particularly laminate-foam sandwich plates, can arise for a certain range of stiffness and geometric parameters, depending on the proper value of parameter m of the Doyle–Ericksen finite strain tensor, as determined in the previous analysis. The bifurcation is symmetric and Koiter's 2/3-power law is followed. The analytical predictions of maximum load reductions due to imperfection sensitivity are verified by finite element simulations. The possibility of interaction between different instability modes, particularly lateral deflection and bulging, is also explored, with the conclusion that lateral deflection dominates in common practical situations.

Keywords: Stability; Finite strain; Critical loads; Postcritical behavior; Imperfection sensitivity; Homogenization; Composites; Sandwich structures; Finite element analysis

* Corresponding author. Tel.: +1 847 491 4025; fax: +1 847 491 4011.
E-mail address: z-bazant@northwestern.edu (Z.P. Bažant).

0020-7683/$ - see front matter © 2005 Elsevier Ltd. All rights reserved.
doi:10.1016/j.ijsolstr.2005.07.040

1. Introduction

The problem of critical loads in buckling of columns deflecting with significant shear deformation, such as sandwich columns, composite columns, lattice columns, helical springs and elastomeric bearings, has been the subject of extensive polemics for several decades. These discussions revolved around the correct choice among various stability theories, each associated with a different finite strain measure.

The best examples of the disputed theories are the formulas of Engesser and Haringx (see details in Bažant, 2003; Bažant and Beghini, 2004, 2005a,b). The polemics were settled in Bažant (1971) by the demonstration that these two formulas are equivalent if the shear modulus is properly transformed as a function of the axial stress. In recent papers (Bažant, 2003; Bažant and Beghini, 2004, 2005a), the energetic variational analysis from Bažant (1971) and Bažant and Cedolin (1991) was extended to light-core sandwich beams buckling in the range of linear material behavior. It was found that a constant tangent (or incremental) shear modulus (as measured, for example, in small-strain torsional tests of a circular tube) can be used only in the Engesser-type theory (associated to the Green's Lagrangian strain, corresponding to the Doyle–Ericksen finite-strain tensor with parameter $m = 2$), and that the Haringx-type theory (associated to the Almansi's Lagrangian strain, corresponding to the Doyle–Ericksen finite-strain tensor with parameter $m = -2$) is usable only if the shear modulus of the core is considered to be a certain linear function of the axial stress in the skins.

The analysis was later extended (Bažant and Beghini, 2005b) to general homogenized orthotropic structures very soft in shear, including layered structures such as elastomeric bearings, which are loaded tranversely to the direction of stiffening plates, and structures loaded in both directions of orthotropy. On one side, the analysis confirmed the applicability of Haringx theory for elastomeric rubber bearings. On the other, it showed that for homogenized biaxially stressed structures the incremental or critical load analysis can utilize a constant small-strain shear modulus if, and only if, one adopts a formulation associated with a general Doyle–Ericksen finite-strain tensor of stress-dependent parameter m.

The analysis of the correct stability theory to be applied for the critical load of structures conducted in these previous papers has been essential to clarify the instability characteristics of several different types of structures. However, it is now crucial to understand whether the critical load will actually be reached by the structure or if there is imperfection sensitivity, which could cause the column to reach a maximum load lower than the critical load.

Therefore, the objective of this paper is to extend the energetic variational analysis conducted in Bažant (2003), Bažant and Beghini (2004, 2005a,b) to the initial postbuckling behavior of homogenized columns accounting for the effect of shear and transverse deformation, explore the consequences for common geometries and material properties, and compare the analytical results to finite element simulations conducted using the commercial software ABAQUS.

Some aspects of the problem addressed in this paper were presented in 1992 by Waas in the context of laminated columns. Here, a similar approach to the one described in Waas (1990, 1992) in the spirit of Koiter (1945) is adopted. Other interesting contributions to the problem for laminated composite beams are presented in the work of Stein (1985, 1989) and Stein and Jegley (1987). Recently, the problem was addressed by Huang and Kardomateas (2000) with reference to sandwich columns.

2. Background on buckling of structures weak in shear

The energetic variational analysis conducted in previous papers (Bažant, 2003; Bažant and Beghini, 2004, 2005a,b) for structures very weak in shear lead to the conclusion that the differences between various stability theories for buckling with shear arise from different choices of the associated finite strain measure. The different measures used in the literature can be represented by using the Doyle–Ericksen finite strain

tensors $\epsilon^{(m)} = (\boldsymbol{U}^m - \boldsymbol{I})/m$ where m = real parameter, $\boldsymbol{I}$ = unit tensor, and $\boldsymbol{U}$ = right-stretch tensor. In particular, $m = 2$ gives Green's Lagrangian strain tensor, and $m = -2$ Almansi's Lagrangian strain tensor.

The stability criteria obtained from any of these strain measures have been shown in Bažant (1971) and Bažant and Cedolin (1991) to be mutually equivalent if the tangent moduli $C^{(m)}_{ijkl}$ associated with different m-values satisfy the relation:

$$C^{(m)}_{ijkl} = C^{(2)}_{ijkl} + \frac{2-m}{4}(S_{ik}\delta_{jl} + S_{jk}\delta_{il} + S_{il}\delta_{jk} + S_{jl}\delta_{ik}) \tag{1}$$

where the subscript indeces $i,j,k,l = 1,2,3$ refer to the components of the tensor in a Cartesian coordinate system, $C^{(2)}_{ijkl}$ are the components of tangent moduli tensor $\boldsymbol{C}^{(m)}$ associated with Green's Lagrangian strain ($m = 2$) and S_{ij} are the components of the current stress tensor $\boldsymbol{S}$ (Cauchy stress). It is of particular interest for later use in this paper to note the expression of the shear modulus C_{1313}:

$$C^{(m)}_{1313} = C^{(2)}_{1313} + \frac{2-m}{4}(S_{11} + S_{33}) \tag{2}$$

By applying this general framework to the problem of buckling of structures weak in shear and analyzing the experimental data available in the literature, it was shown in Bažant (2003), Bažant and Beghini (2004, 2005a,b) that:

- The stability theory based on Green's Lagrangian strain ($m = 2$) is associated with Engesser's formula while Almansi's Lagrangian strain ($m = -2$) is associated with Haringx's formula.
- The two formulas are related according to Eq. (2), i.e., one follows from the other.
- Engesser's formula can be used (with constant C_{1313}) for structures reinforced in the direction of the applied load (e.g., sandwich structures) while Haringx's can be used for structures reinforced transversely to the load direction (e.g., elastomeric rubber bearings).
- Commercial finite element software, which is based on an updated Lagrangian formulation, can correctly capture the Engesser load if the shear modulus is kept constant. The Haringx load (or any other load associated with a certain value of the parameter m) of homogenized structures is obtained if, at each step of the computation, the shear modulus of the core is properly updated according to the current axial stress in the skins, or if the finite element program is generalized to a variational principle corresponding to the correct value of parameter m.

In relation to these previous studies, a further step is now taken to investigate the imperfection sensitivity by extending the analysis to the initial postcritical behavior of the structure.

3. Variational analysis of the initial postcritical behavior of homogenized orthotropic columns

Let us consider a homogenized orthotropic column of length L under the assumptions of plane cross section and inextensibility of the centroidal line (see Fig. 1). The overall thickness of the column is h, and the width $b = 1$. In line with the assumptions in Waas (1990, 1992), rigorously justified in Stoker (1968) and Novozhilov (1953), the kinematic model used to describe the column in large deformation is given by

$$U(X,Z) = U_0(X) - Z\frac{\mathrm{d}\Psi_0}{\mathrm{d}X}, \quad W(X,Z) = W_0(X) + Z\frac{\mathrm{d}U_0}{\mathrm{d}X} \tag{3}$$

where X and Z are Lagrangian coordinates (see Fig. 1a), $U(X,Z)$, $W(X,Z)$ are the displacement of a point in X and Z direction, respectively, $U_0(X)$ and $W_0(X)$ are the displacements of the centroidal line in

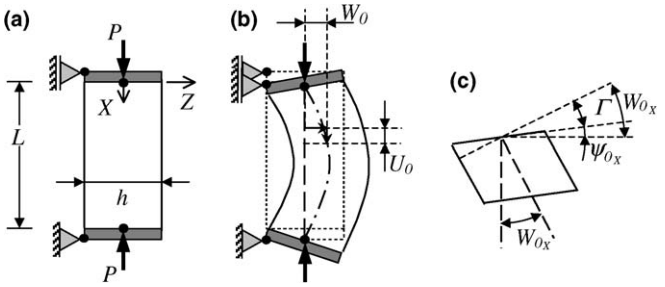

Fig. 1. (a) Column in the initial state; (b) displacement field after buckling; (c) shear deformation in the cross section.

directions X and Z, respectively (see Fig. 1b), and $\mathrm{d}\Psi_0/\mathrm{d}X$ is the rotation of the cross section (see Fig. 1c). Consequently, the shear angle Γ is given by $\mathrm{d}W_0/\mathrm{d}X - \mathrm{d}\Psi_0/\mathrm{d}X$, and the inextensibility condition for the centroidal line of the beam can be written as

$$\left(\frac{\mathrm{d}U_0}{\mathrm{d}X}+1\right)^2+\left(\frac{\mathrm{d}W_0}{\mathrm{d}X}\right)^2-1=0 \tag{4}$$

The kinematic model in Eq. (3) is very similar to that considered in traditional small-strain beam theory, the only difference being the term $Z\,\mathrm{d}U_0/\mathrm{d}X$ in the expression for $W(X,Z)$. This is related to the deformation in transverse direction Z, typically neglected in small-strain analysis but important for the postcritical behavior of the structure.

Let us now consider the Green's Lagrangian strain, which corresponds to the Doyle–Ericksen finite strain tensor of order $m=2$ and whose component form reads:

$$\epsilon_{ij}^{(2)}=\frac{1}{2}\left(\frac{\partial U_i}{\partial X_j}+\frac{\partial U_j}{\partial X_i}+\frac{\partial U_k}{\partial X_i}\frac{\partial U_k}{\partial X_j}\right) \tag{5}$$

Here, summation over the repeated index k is implied and $U_1=U_0$, $U_2=W_0$, $X_1=X$, $X_2=Z$. If the kinematic model in Eq. (3) is substituted in Eq. (5) and the inextensibility condition (4) is considered, the expression for the strain becomes as follows:

$$\begin{aligned}
\epsilon_{XX}^{(2)}&=-Z\left[\frac{\Psi_{XX}+W_X^2(W_{XX}-\Psi_{XX})}{\sqrt{1-W_X^2}}\right]+\frac{Z^2}{2}\left[\frac{\Psi_{XX}+W_X^2(W_{XX}^2-\Psi_{XX}^2)}{1-W_X^2}\right]\\
\epsilon_{ZZ}^{(2)}&=\frac{1}{2}(\Psi_X^2-W_X^2)\\
\epsilon_{XZ}^{(2)}&=\frac{1}{2}(W_X-\Psi_X)\sqrt{1-W_X^2}+\frac{Z}{4}\frac{\mathrm{d}}{\mathrm{d}X}(\Psi_X^2-W_X^2)
\end{aligned} \tag{6}$$

In the above expressions and in what follows, the subscript 0 referring to the centroidal line is dropped for convenience and the notations $\mathrm{d}f/\mathrm{d}X=f_X$, $\mathrm{d}^2f/\mathrm{d}X^2=f_{XX}$, etc. are introduced for any function f. Note that, if the cross section stays perpendicular to the centroidal line (i.e., $W_X=\Psi_X$), Eq. (6) reduces to the classical Euler–Bernoulli formulation since $\epsilon_{ZZ}^{(2)}=0$ and $\epsilon_{XZ}^{(2)}=0$.

The elastic constitutive model for the two-dimensional problem of buckling and postbuckling can now be written using the second Piola–Kirchhoff stress $\Sigma_{ij}^{(2)}$ (energetically conjugate to the Green's Lagrangian strain) and neglecting the Poisson effect as suggested in Waas (1992) (and references therein):

$$\Sigma_{XX}^{(2)} = E_{XX}^{(2)}\epsilon_{XX}^{(2)} \quad \Sigma_{ZZ}^{(2)} = E_{ZZ}^{(2)}\epsilon_{ZZ}^{(2)} \quad \Sigma_{XZ}^{(2)} = G_{XZ}^{(2)}\epsilon_{XZ}^{(2)} \tag{7}$$

where $E_{XX}^{(2)}$, $E_{ZZ}^{(2)}$, $G_{XZ}^{(2)}$ are, respectively, the longitudinal, transverse and shear stiffness of the homogenized column considered with respect to the Green's Lagrangian strain measure.

Coherently with the conclusions in Bažant (2003), Bažant and Beghini (2004, 2005a,b), which are summarized in the previous paragraph, the expression for the potential energy corresponding to a general value of the parameter m in the Doyle–Ericksen formula can be written considering the Green's Lagrangian strain (5) and using Eq. (2) for the shear modulus;

$$\begin{aligned}\Pi &= \frac{1}{2}\int_0^L \int_A \left[C_{1111}^{(m)}(\epsilon_{XX}^{(m)})^2 + C_{3333}^{(m)}(\epsilon_{ZZ}^{(m)})^2 + 2C_{1313}^{(m)}(\epsilon_{XZ}^{(m)})^2\right] \mathrm{d}A\,\mathrm{d}X + P\int_0^L \frac{\mathrm{d}U_0}{\mathrm{d}X}\mathrm{d}X \\ &= \frac{1}{2}\int_0^L \int_A \left\{E_{XX}^{(2)}(\epsilon_{XX}^{(2)})^2 + E_{ZZ}^{(2)}(\epsilon_{ZZ}^{(2)})^2 + 2\left[G_{XZ}^{(2)} + \frac{2-m}{4}S_{11}\right](\epsilon_{XZ}^{(2)})^2\right\}\mathrm{d}A\,\mathrm{d}X + P\int_0^L \frac{\mathrm{d}U_0}{\mathrm{d}X}\mathrm{d}X\end{aligned} \tag{8}$$

where it is assumed that $C_{1111}^{(m)} = E_{XX}^{(m)} = C_{1111}^{(2)} + (2-m)S_{11} \approx E_{XX}^{(2)}$ because usually $C_{1111}^{(2)} \gg S_{11}$, while $C_{3333}^{(m)} = E_{ZZ}^{(m)} = C_{3333}^{(2)} + (2-m)S_{33} \approx E_{ZZ}^{(2)}$ and $C_{1313}^{(m)} = G_{XZ}^{(m)} = C_{1313}^{(2)} + \frac{2-m}{4}(S_{11}+S_{33}) \approx G_{XZ}^{(2)} + \frac{2-m}{4}S_{11}$ because $C_{3333}^{(2)} \gg S_{33}$ and $C_{1313}^{(2)} \gg S_{33}$ for the problem of column buckling under consideration.

Eq. (6) can now be substituted in expression (8) for the potential energy;

$$\begin{aligned}\Pi = {} & \frac{E_{XX}I}{2}\int_0^L \left[\Psi_{XX}^2\left(1-W_X^2\right) + 2\Psi_{XX}W_{XX}W_X^2\right]\mathrm{d}X + \frac{E_{ZZ}h}{8}\int_0^L \left(\Psi_X^2 - W_X^2\right)^2\mathrm{d}X \\ & + \frac{\kappa G_{XZ}^{(m)}I}{2}\int_0^L \left(W_X W_{XX} - \Psi_X\Psi_{XX}\right)^2\mathrm{d}X + \frac{\kappa G_{XZ}^{(m)}h}{2}\int_0^L \left(W_X - \Psi_X\right)^2\left(1-W_X^2\right)\mathrm{d}X \\ & - \frac{P}{2}\int_0^L \left(W_X^2 + \frac{1}{4}W_X^4\right)\mathrm{d}X\end{aligned} \tag{9}$$

In the foregoing expression, κ is related to the reduced cross section ($\kappa = 5/6$ for rectangular cross section), the series expansion for the square root is introduced for Eq. (4) as $\mathrm{d}U_0/\mathrm{d}X = \sqrt{1-W_X^2} - 1 \approx -\frac{1}{2}[W_X^2 + W_X^4/4]$, the notation $\int_{-h/2}^{h/2} Z^2\,\mathrm{d}Z = I$ is considered for the inertia of the cross section, and superscript (2) is dropped from the stiffness moduli for convenience. In Eq. (9) only terms up to the fourth-order are included and some of these fourth-order terms are neglected because of no influence on the results.

The following dimensionless variables are now introduced:

$$\begin{aligned}&x = \frac{X}{L}, \quad w = \frac{W}{L}, \quad \psi = \frac{\Psi}{L}, \quad \beta = \frac{L^2E_{ZZ}h}{4E_{XX}I}, \quad \delta^{(m)} = \frac{\kappa L^2 G_{XZ}^{(m)}h}{E_{XX}I}, \\ &\eta = \frac{L}{h}, \quad \gamma^{(m)} = \frac{\kappa G_{XZ}^{(m)}}{E_{XX}}, \quad \sigma = \frac{PL^2}{4E_{XX}I}, \quad \Pi^* = \frac{2\Pi L}{E_{XX}I}\end{aligned}$$

Note that

$$\begin{aligned}&\frac{\mathrm{d}W}{\mathrm{d}X} = \frac{\mathrm{d}w}{\mathrm{d}x}, \quad \frac{\mathrm{d}^2W}{\mathrm{d}X^2} = \frac{1}{L}\frac{\mathrm{d}^2w}{\mathrm{d}x^2}, \quad \frac{\mathrm{d}\Psi}{\mathrm{d}X} = \frac{\mathrm{d}\psi}{\mathrm{d}x}, \quad \frac{\mathrm{d}^2\Psi}{\mathrm{d}X^2} = \frac{1}{L}\frac{\mathrm{d}^2\psi}{\mathrm{d}x^2}, \\ &\delta^{(m)} = \delta^{(2)} + (2-m)\sigma, \quad \gamma^{(m)} = \gamma^{(2)} + \frac{2-m}{12}\frac{\sigma}{\eta^2}\end{aligned}$$

Therefore, Eq. (9) becomes:

$$\Pi^* = \int_0^1 \left[\psi_{xx}^2\left(1-w_x^2\right) + 2\psi_{xx}w_{xx}w_x^2\right]\mathrm{d}x + \beta\int_0^1 \left(\psi_x^2 - w_x^2\right)^2\mathrm{d}x + \gamma^{(m)}\int_0^1 (w_x w_{xx} - \psi_x\psi_{xx})^2\mathrm{d}x + \delta^{(m)}\int_0^1 (w_x-\psi_x)^2\left(1-w_x^2\right)\mathrm{d}x - 4\sigma\int_0^1 \left(w_x^2 + \frac{1}{4}w_x^4\right)\mathrm{d}x \tag{10}$$

The governing equations of the problem of buckling and initial postbuckling are now obtained by imposing the condition that the first variation of the potential energy is zero for any kinematically admissible variation δw and $\delta\psi$ (Trefftz condition, Bažant and Cedolin, 1991):

$$\delta\Pi^* = \int_0^1 [F(w,\psi)\delta w + H(w,\psi)\delta\psi]\mathrm{d}x + \text{boundary conditions} = 0 \tag{11}$$

Because this must be satisfied for any variations δw and $\delta\psi$, we obtain two coupled equations describing the problem:

$$\begin{aligned} F(w,\psi) = {} & 2(\psi_{xx}^2 w_x)_x + 2(\psi_{xx}w_x^2)_{xx} - 4(w_x w_{xx}\psi_{xx})_x - 4\beta[w_x(w_x^2-\psi_x^2)]_x \\ & - 2\delta^{(m)}\left[-w_x(w_x-\psi_x)^2 + (1-w_x^2)(w_x-\psi_x)\right]_x + 2\gamma^{(m)}[w_x(w_x w_{xx} - \psi_x\psi_{xx})]_{xx} \\ & + 2\gamma^{(m)}(\psi_x\psi_{xx}w_{xx} - w_x w_{xx}^2)_x + 4\sigma(2w_x + w_x^3)_x = 0 \end{aligned} \tag{12}$$

$$\begin{aligned} H(w,\psi) = {} & 2[\psi_{xx}(1-w_x^2)]_{xx} + 2(w_x^2 w_{xx})_{xx} - 4\beta[\psi_x(\psi_x^2 - w_x^2)]_x + 2\delta^{(m)}[(w_x-\psi_x)(1-w_x^2)]_x \\ & + 2\gamma^{(m)}(\psi_x^2\psi_{xx} - w_x w_{xx}\psi_x)_{xx} - 2\gamma^{(m)}(\psi_x\psi_{xx}^2 - w_x w_{xx}\psi_{xx})_x = 0 \end{aligned} \tag{13}$$

Eqs. (12) and (13) must be solved considering the proper boundary conditions for the unknown functions w and ψ. These equations involve only linear terms and third-order terms, due to the fact that only terms up to the fourth-order have been considered in Eq. (10). If the equations are truncated after the linear terms, we obtain Eqs. (22), (23) in Bažant (2003), which were used to compute the critical load for a general m. Therefore, the higher order terms included here are specifically related to the initial postcritical behavior of the structure.

Note that the trivial solution $w(x) = 0$ and $\psi(x) = 0$ satisfies Eqs. (12) and (13) for any value of the load σ. However, we are interested in the non-trivial solution (i.e., the eigenfunctions) corresponding to the buckling load of the structure σ_{cr}. Let us now perturb the governing equations near this non-trivial buckling solution according to the general approach introduced by Koiter (1945):

$$\begin{aligned} \sigma &= \sum_{n=0}^{\infty}\epsilon^n\sigma_n = \sigma_0 + \epsilon\sigma_1 + \epsilon^2\sigma_2 + \cdots \\ w(x) &= \sum_{n=1}^{\infty}\epsilon^n w_n = \epsilon w_1(x) + \epsilon^2 w_2(x) + \cdots \\ \psi(x) &= \sum_{n=1}^{\infty}\epsilon^n\psi_n = \epsilon\psi_1(x) + \epsilon^2\psi_2(x) + \cdots \end{aligned} \tag{14}$$

where $\sigma_0 = \sigma_{cr}$ is the first critical load of the structure, and ϵ is a perturbation parameter such that ϵ^n amplifies the buckling mode (w_n, ψ_n) corresponding to the load σ_n $(n = 1, 2, 3, \ldots)$. If expressions (14) are substituted in Eqs. (12) and (13) and the terms are conveniently grouped, we obtain:

$$\begin{aligned} \frac{1}{2}F(w,\psi) &= \sum_{n=1}^{\infty}[L_1(w_n,\psi_n) - R_n]\epsilon^n = 0 \\ \frac{1}{2}H(w,\psi) &= \sum_{n=1}^{\infty}[L_2(w_n,\psi_n) - Q_n]\epsilon^n = 0 \end{aligned} \tag{15}$$

where

$$L_1(w_n,\psi_n) = (4\sigma_{cr} - \delta_0^{(m)})w_{n_{xx}} + \delta_0^{(m)}\psi_{n_{xx}}$$
$$L_2(w_n,\psi_n) = \delta_0^{(m)}w_{n_{xx}} + \psi_{n_{xxxx}} - \delta_0^{(m)}\psi_{n_{xx}} \quad n = 1,2,3,\ldots$$
$$\delta_0^{(m)} = \delta^{(2)} + (2-m)\sigma_{cr}$$

and

$$R_1 = 0 \quad Q_1 = 0$$
$$R_2 = -4\sigma_1 w_{1_{xx}} + \sigma_1(2-m)(w_{1_{xx}} - \psi_{1_{xx}})$$
$$Q_2 = -\sigma_1(2-m)(w_{1_{xx}} - \psi_{1_{xx}})$$
$$\begin{aligned} R_3 = {} & -(\psi_{1_{xx}}^2 w_{1_x})_x - (\psi_{1_{xx}} w_{1_x}^2)_{xx} + 2(w_{1_x} w_{1_{xx}} \psi_{1_{xx}})_x + 2\beta[w_{1_x}(w_{1_x}^2 - \psi_{1_x}^2)]_x \\ & + \delta_0^{(m)}\left[-2w_{1_x}^3 + (3w_{1_x} - \psi_{1_x})w_{1_x}\psi_{1_x}\right]_x - \gamma_0^{(m)}[w_{1_x}(w_{1_x}w_{1_{xx}} - \psi_{1_x}\psi_{1_{xx}})]_{xx} \\ & - \gamma_0^{(m)}(\psi_{1_x}\psi_{1_{xx}}w_{1_{xx}} - w_{1_x}w_{1_{xx}}^2)_x - 2\sigma_{cr}(w_{1_x}^3)_x - 4\sigma_1 w_{2_{xx}} \\ & - 4\sigma_2 w_{1_{xx}} + \sigma_2(2-m)(w_{1_{xx}} - \psi_{1_{xx}}) + \sigma_1(2-m)(w_{2_{xx}} - \psi_{2_{xx}}) \end{aligned}$$
$$\begin{aligned} Q_3 = {} & (\psi_{1_{xx}} w_{1_x}^2)_{xx} - (w_{1_x}^2 w_{1_{xx}})_{xx} + 2\beta[\psi_{1_x}(\psi_{1_x}^2 - w_{1_x}^2)]_x - \delta_0^{(m)}[-w_{1_x}^2(w_{1_x} - \psi_{1_x})]_x \\ & - \gamma_0^{(m)}(\psi_{1_x}^2\psi_{1_{xx}} - w_{1_x}w_{1_{xx}}\psi_{1_x})_{xx} + \gamma_0^{(m)}(\psi_{1_x}\psi_{1_{xx}}^2 - w_{1_x}w_{1_{xx}}\psi_{1_{xx}})_x \\ & - \sigma_2(2-m)(w_{1_{xx}} - \psi_{1_{xx}}) \end{aligned}$$

In the foregoing expressions $\gamma_0^{(m)} = \gamma^{(2)} + (2-m)\sigma_{cr}$ and $w_{n_x} = \mathrm{d}w_n/\mathrm{d}x, w_{n_{xx}} = \mathrm{d}^2 w_n/\mathrm{d}x^2$, etc. The coupled set of equations in Eq. (15) for each power $n = 1,2,3,\ldots$ of the perturbation parameter ϵ can be simplified by eliminating one of the two functions. In particular, if we eliminate ψ, we obtain:

$$L_3(w_n) = \delta(R_n + Q_n) - R_{n_{xx}} \tag{16}$$

where

$$L_3(w_n) = (\delta^{(m)} - 4\sigma_{cr})w_{n_{xxxx}} + 4\sigma_{cr}\delta^{(m)}w_{n_{xx}} \tag{17}$$

Eq. (16) must be solved for the proper boundary conditions on function w_n. The solutions of (16) for increasing values of the power n are associated with different aspects of the buckling and postbuckling of the column. In particular, for $n = 1$ we obtain the buckling characteristics of the structure, $n = 2$ does not give any contribution and $n = 3$ describes the initial postbuckling.

4. Solution of the governing equation for various boundary conditions

4.1. Buckling load ($n = 1$)

For the case $n = 1$, Eq. (16) reduces to the problem of buckling of structures weak in shear analyzed in Bažant (2003), Bažant and Beghini (2004, 2005a,b). The general solution of the governing equations (15) associated with the first power of ϵ reads:

$$\begin{aligned} w_1(x) &= A\sin x + B\cos x + Cx + D \\ \psi_1(x) &= \hat{A}\sin x + \hat{B}\cos x + \hat{C}x + \hat{D} \end{aligned} \tag{18}$$

To relate the constants in Eq. (18), we define the parameter:

$$s^{(m)} = \frac{\delta^{(2)} - (2+m)\sigma_{cr}^{(m)}}{\delta^{(2)} + (2-m)\sigma_{cr}^{(m)}} \tag{19}$$

Table 1
Eigenfunctions for different boundary conditions

Name	Conditions	$w_1(x)/q$	α	q
Pinned–pinned	$w(0) = w(1) = 0$ $\psi_{xx}(0) = \psi_{xx}(1) = 0$	$\sin \pi x$	1	ϵ
Clamped–clamped	$w(0) = w(1) = 0$ $\psi_x(0) = \psi_x(1) = 0$	$1 - \cos 2\pi x$	0.5	$\epsilon/2$
Clamped–free	$w(0) = 0$, $sw_x(1) = \psi_x(1)$ $\psi_x(0) = \psi_{xx}(1) = 0$	$1 - \cos\frac{\pi x}{2}$	2	ϵ
Sliding–clamped	$w(1) = 0$, $sw_x(0) = \psi_x(0)$ $\psi_x(0) = \psi_x(1) = 0$	$1 + \cos \pi x$	1	$\epsilon/2$
Sliding–pinned	$w(1) = 0$, $sw_x(0) = \psi_x(0)$ $\psi_x(0) = \psi_{xx}(1) = 0$	$\cos\frac{\pi x}{2}$	2	ϵ

Then we can write $\hat{A} = s^{(m)}A$ and $\hat{B} = s^{(m)}B$, because $\psi_{1_{xx}} = s^{(m)}w_{1_{xx}}$ from Eq. (15) for $n = 1$. Note that expression (19) is equivalent to Eq. (26) in Bažant (2003). For all the boundary conditions in Table 1, it can be also shown that $\psi_{1_x} = s^{(m)}w_{1_x}$. Exploiting this result and observing that $w_{1_{xxxx}} = -p^2 w_{1_{xx}}$ where $p = \pi^2/\alpha^2$, with $\alpha L =$ effective length of the column (see Table 1), we obtain the following expression for the critical load from $L_3(w_1) = 0$:

$$p^2 = \frac{4\sigma_{\mathrm{cr}}\delta^{(m)}}{\delta^{(m)} - 4\sigma_{\mathrm{cr}}} \tag{20}$$

Rearranging the terms

$$(2-m)\sigma_{\mathrm{cr}}^2 + \sigma_{\mathrm{cr}}[\delta^{(2)} + \sigma_{\mathrm{E}}(m+2)] - \delta^{(2)}\sigma_{\mathrm{E}} = 0 \tag{21}$$

where $\sigma_{\mathrm{E}} = P_{\mathrm{E}}L^2/(4EI) = p^2/4$ is the Euler load of the column. The solution of Eq. (21) gives us the critical load of the column as

$$\sigma_{\mathrm{cr}}^{(m)} = \frac{\delta^{(2)} + \sigma_{\mathrm{E}}(m+2)}{2(2-m)}\left\{\sqrt{1 + \frac{4\delta^{(2)}\sigma_{\mathrm{E}}(2-m)}{[\delta^{(2)} + \sigma_{\mathrm{E}}(2+m)]^2}} - 1\right\} \quad (m \neq 2) \tag{22}$$

$$\sigma_{\mathrm{cr}}^{(2)} = \frac{\delta^{(2)}\sigma_{\mathrm{E}}}{\delta^{(2)} + 4\sigma_{\mathrm{E}}} \quad (m = 2) \tag{23}$$

The above expressions coincide with Eqs. (5) and (6) in Bažant and Beghini (2005b) independently of the boundary conditions considered. Therefore, the results obtained in the previous papers (Bažant, 2003; Bažant and Beghini, 2004, 2005a,b) with neglect of the transverse stiffness are still perfectly valid since the transverse stiffness affects only terms of order higher than the second. On the other hand, it plays a fundamental role in the initial postcritical behavior of the structure as shown in what follows.

4.2. Zero contribution ($n = 2$)

The set of equations associated with the second power of the perturbation parameter makes no contribution to the load–deflection solution for any boundary condition. This can be proven by writing Eq. (16) for $n = 2$ as

$$(\delta^{(m)} - 4\sigma_{cr})w_{2_{xxxx}} + 4\sigma_{cr}\delta^{(m)}w_{2_{xx}} = \sigma_1[-4\delta^{(m)}w_{1_{xx}} + 4w_{1_{xxxx}} + (m-2)(w_{1_{xxxx}} - \psi_{1_{xxxx}})] \tag{24}$$

This equation is solved by superposing the solution of the homogeneous equation $L_3(w_2) = 0$, which implies $w_2 = w_1$, and a particular integral w_{2p} obtained by considering the right-hand side of (24). This is a combination of trigonometric functions because of the general solution given by Eq. (18) for w_1 and ψ_1. Therefore, the particular solution w_{2p} is chosen to be a combination of trigonometric functions similar to w_1. Consequently, the left-hand side is zero since $L_3(w_1) = 0$ and the only possibility for the right hand side to be zero is that $\sigma_1 = 0$. This verifies that the second power of the perturbation parameter does not contribute to the load–displacement curve of a column for any boundary condition.

4.3. Initial postcritical behavior ($n = 3$)

The solution of the coupled equations (15) associated with $n = 3$ describes the initial postcritical behavior of the structure considered. As a reference case for later comparisons, consider first the simpler problem of initial postbuckling of Euler–Bernoulli columns, when the cross section is considered rigid and the shear deformation is negligible, i.e., $w(x) = \psi(x)$, $s^{(m)} = 1$, and $\delta \to \infty$. In this case the potential energy can be simply written as (Bažant and Cedolin, 1991):

$$\Pi^* = \int_0^1 w_{xx}^2 \,\mathrm{d}x - 4\sigma \int_0^1 \left(w_x^2 - \frac{1}{12}w_x^4\right)\mathrm{d}x \tag{25}$$

The initial postcritical behavior is obtained by assuming function $w(x)$ in the above expression to be equal to the first eigenfunction of the buckling problem. Substituting in Eq. (25) the expression of w_1 reported in Table 1 for various boundary conditions, and imposing the condition of vanishing first variation of Π^* with respect to the amplification parameter q, we obtain:

$$\frac{\sigma}{\sigma_{cr}} = 1 + \frac{(pq)^2}{8} \tag{26}$$

It is interesting to note that this simple formula describes the initial postcritical behavior of Euler–Bernoulli columns for all the boundary conditions in Table 1. The effect of each boundary condition is given, in this formula, by the parameter $p = \pi/\alpha$, and the amplification parameter q must be properly scaled according to ϵ, as indicated in Table 1. This is necessary because the perturbation parameter ϵ is assumed to amplify the maximum displacement along the beam axis.

Let us now go back to the initial postcritical behavior of homogenized structures including shear and transverse deformability, and solve the third-order terms of Eq. (15). The expression obtained for the right hand side of Eq. (16) is slightly complicated, in particular for the case of general m. Therefore, a computer program using symbolic software has been used to carry out the calculations. In general, the right hand side for the different boundary conditions can be expressed as a sum of orthogonal functions:

$$L_3(w_3) = \delta(R_3 + Q_3) - R_{3_{xx}} = T_1 \cos px + T_2 \cos 2px \tag{27}$$

To satisfy this equation, we need to suppress the term T_1, which will give the expression for σ_2, while the term T_2 is related to the coefficients in the expression for w_3. For $m = 2$, the resulting expression for σ_2 (valid for sandwich columns, lattice columns, etc.) is given by

$$\sigma_2 = \frac{p^4q^2}{32(p^2+\delta)^4}[\delta^4 - 5\delta^3p^2 + \delta^2(16p^4\gamma + 48p^2\beta - 13p^4) + \delta(16p^6\gamma + 48p^4\beta - 7p^6) + 4p^8\gamma + 12p^6\beta] \tag{28}$$

where, for the sake of brevity, the superscript (2) has been dropped. This expression is valid for any boundary condition indicated in Table 1. The user needs only to define the proper value of the parameters according to the given materials, geometry and boundary conditions. It is noted immediately that for $\delta \to \infty$:

$$\frac{\sigma_2}{\sigma_{cr}} \to \frac{(pq)^2}{8} \tag{29}$$

This agrees with Eq. (26) and thus confirms the validity of Eq. (28).

Eq. (28) can be extended to the case of general m as follows:

$$\sigma_2 = \left(K_1\sigma_0^4 + K_2\sigma_0^3 + K_3\sigma_0^2 + K_4\sigma_0 + K_5\right)/K_6 \tag{30}$$

where

$$\begin{aligned}
K_1 &= -4p^4m^2 - \frac{9}{2}p^2\eta m^3 + 180p^2\eta + 63p^2\eta m^2 - 198p^2\eta m + 8mp^4\\
K_2 &= 144m\beta p^2\eta + \frac{9}{2}m^2p^4\eta + 2mp^6 - m^2p^6 + \frac{3}{2}m^3p^4\eta + 138p^4\eta - 8p^4\delta + \frac{27}{2}p^2\eta m^2\delta\\
&\quad + 48p^4m\gamma\eta - 126p^2\eta m\delta - 84mp^4\eta + 198p^2\eta\delta + 4p^4\delta m\\
K_3 &= -9p^4\eta m\delta + 84p^4\eta\delta + 12p^6\eta - 144\beta p^2\eta\delta - \frac{3}{2}m^2p^6\eta + mp^6\delta\\
&\quad - 2p^6\delta + 63p^2\eta\delta^2 + 36p^4\beta\eta m - 48p^4\gamma\eta\delta + 3mp^6\eta - \frac{27}{2}p^2\eta m\delta^2 + 12mp^6\gamma\eta - \frac{9}{2}m^2p^4\eta\delta\\
K_4 &= -12p^6\gamma\eta\delta - 36p^4\beta\eta\delta + 3mp^6\eta\delta + \frac{9}{2}p^4\eta\delta^2 + \frac{9}{2}p^2\eta\delta^3 - 3p^6\eta\delta + \frac{9}{2}mp^4\eta\delta^2\\
K_5 &= -\frac{3}{2}p^6\eta\delta^2 - \frac{3}{2}p^4\eta\delta^3\\
K_6 &= 12\eta(\sigma_0 m - 2\sigma_0 - \delta)(\sigma_0^2m^2 - 4m\sigma_0^2 - 2\sigma_0 m\delta + 4\sigma_0^2 + 4\delta\sigma_0 + \delta^2 + p^2\delta)
\end{aligned}$$

Eq. (30) is valid again for any boundary condition in Table 1, each characterized by a certain value of parameter p. The generality of this expression makes it a useful tool to verify numerical solutions by finite elements or similar methods.

5. Parametric study and identification of imperfection sensitive cases

Several combinations of parameters in Eqs. (28) and (30) are considered to investigate the imperfection sensitivity of a homogenized orthotropic column; this sensitivity being characterized by a negative value for the expression of σ_2. The results of the parametric study are shown in Figs. 2–5 in terms of the dimensionless variables G_{XZ}/E_{XX}, E_{ZZ}/E_{XX} and σ_2/σ_0.

For $p = 2\pi$ (clamped–clamped columns), $L/h = 5$ and $m = 2$ (sandwich and lattice columns, etc.), Fig. 2 shows that the structure exhibits imperfection sensitivity for a wide range of values of G_{XZ}/E_{XX} and E_{ZZ}/E_{XX} (see the white region in the figure). This sensitivity disappears quickly for more slender structures, as Fig. 3 documents for the case of $L/h = 10$ and $m = 2$. For the short column shown in Fig. 2, several load–deflection curves corresponding to different values of E_{ZZ}/E_{XX} are depicted in Fig. 6 (note that this column has no initial imperfection).

If the parameter m is changed to $m = 1$ (Biot's strain measure), the imperfection sensitivity appears again for short columns (see Fig. 4). For $m = -2$ (Almansi's Lagrangian strain, valid for helical springs, elastomeric rubber bearings, etc.), there is no imperfection sensitivity, as Fig. 5 shows.

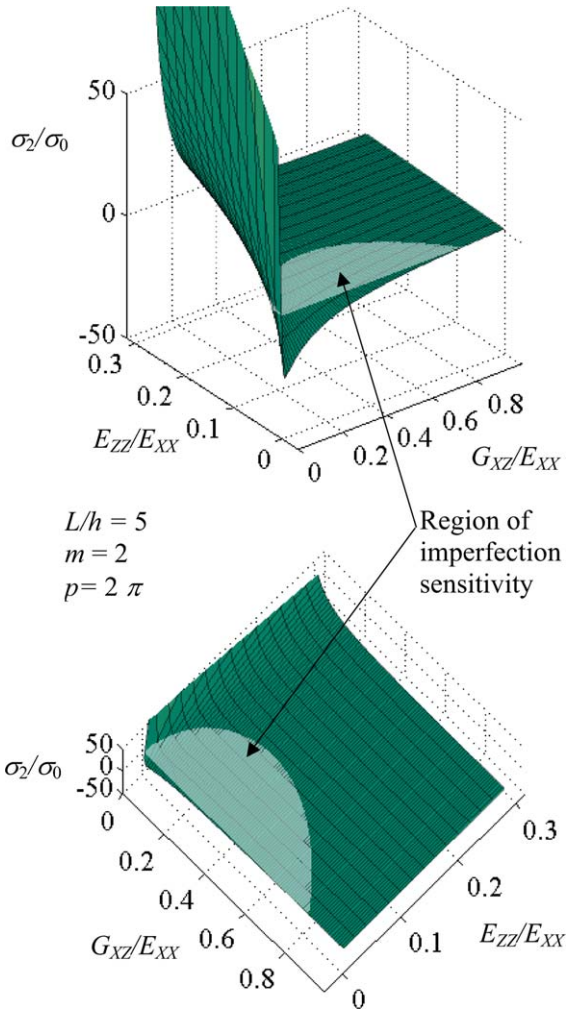

Fig. 2. Imperfection sensitivity for a short column clamped at both ends and $m = 2$.

For $p = \pi$ (pinned–pinned or sliding–clamped column), $L/h = 5$ and $m = 2$, the region of parameters giving imperfection sensitivity is very small and it includes only transverse and shear stiffness values very close to zero. For more slender columns (i.e., higher L/h) or different values of the parameter m, the imperfection sensitivity disappears completely.

For $p = \pi/2$ (clamped–free column), there is no sign of imperfection sensitivity for any combination of parameters considered.

6. Effect of imperfections on column maximum load

So far, the analysis dealt with perfect columns. However, to understand the effect of imperfection sensitivity on the maximum load a column can carry, initial imperfections must be considered. As indicated in Waas (1992) (and references therein), this can be simply done by replacing expansion (14) for σ with:

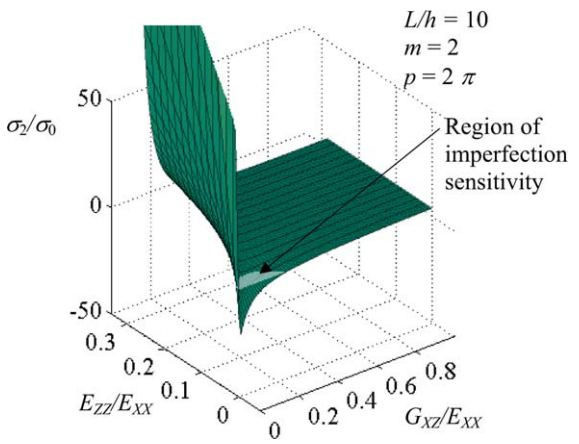

Fig. 3. Imperfection sensitivity for a slender column clamped at both ends and $m = 2$.

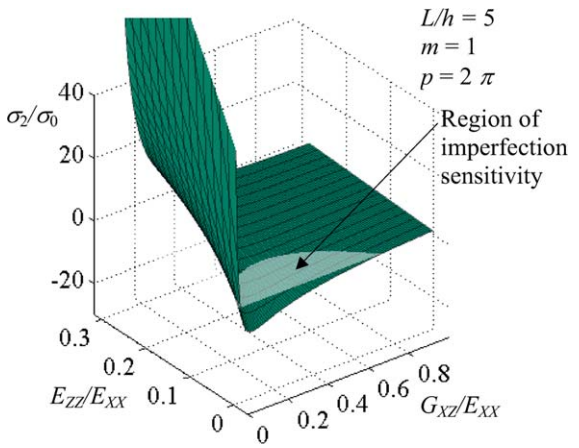

Fig. 4. Imperfection sensitivity for a short column clamped at both ends and $m = 1$.

$$\sigma\bar{\epsilon} = (\sigma_0 - \sigma)\epsilon + \epsilon^2\sigma_1 + \epsilon^3\sigma_2 + \cdots \tag{31}$$

where $\sigma_1 = 0$, as proven earlier, and $\bar{\epsilon}$ is the level of imperfection in the column measured with respect to its buckling mode . Therefore, the load deflection relation becomes:

$$\frac{\sigma}{\sigma_0} = \frac{\epsilon}{\epsilon + \bar{\epsilon}} + \frac{\sigma_2}{\sigma_0}\frac{\epsilon^3}{\epsilon + \bar{\epsilon}} \tag{32}$$

In the case of $\sigma_2 < 0$ (i.e., an imperfection sensitive structure), this equation gives a maximum load (for small $\bar{\epsilon}$) at:

$$\epsilon_{\max} = \left(-\frac{\sigma_0}{\sigma_2}\frac{\bar{\epsilon}}{2}\right)^{1/3} \tag{33}$$

Substituting this into Eq. (32), and using the series expansion:

$$\frac{\epsilon_{\max}}{\epsilon_{\max} + \bar{\epsilon}} = \left(1 + \frac{\bar{\epsilon}}{\epsilon_{\max}}\right)^{-1} = 1 - \frac{\bar{\epsilon}}{\epsilon_{\max}} + \cdots \tag{34}$$

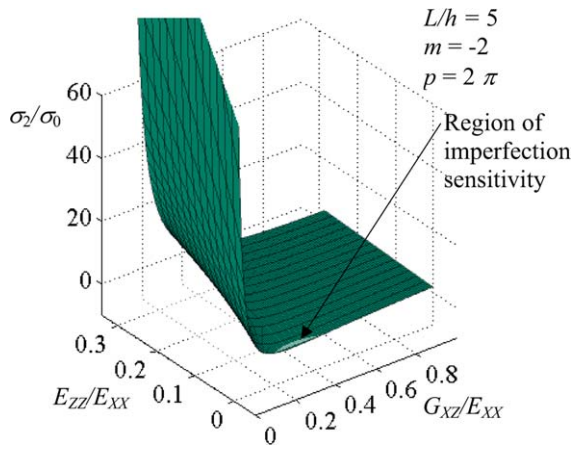

Fig. 5. Imperfection sensitivity for a short column clamped at both ends and $m = -2$.

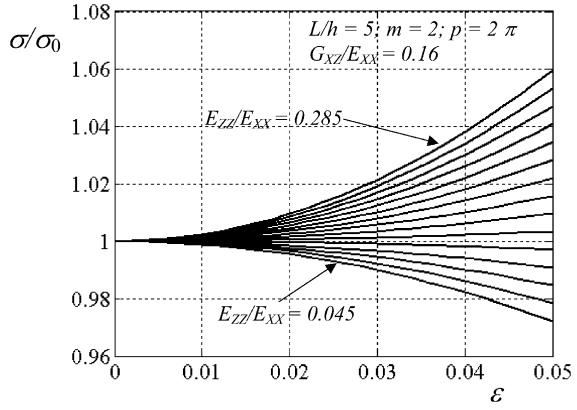

Fig. 6. Postcritical behavior for a short column clamped at both ends and $m = 2$.

we finally obtain:

$$\frac{\sigma_{\max}}{\sigma_0} = 1 - 3\left(-\frac{\sigma_2}{4\sigma_0}\right)^{1/3}(\bar{\epsilon})^{2/3} \tag{35}$$

This expression agrees with Koiter's 2/3-power law.

The effect of the imperfection $\bar{\epsilon}$ on the maximum load of a column is depicted in Fig. 7. The column is considered to be characterized by $m = 2$, $L/h = 5$, $E_{ZZ}/E_{XX} = 0.045$ and $G_{XZ}/E_{XX} = 0.16$. These properties correspond to the ratio $\sigma_2/\sigma_0 = -6.1504$, as calculated from Eq. (28). The lines in Fig. 7 are the plots of Eq. (32) for different values of $\bar{\epsilon}$, while the circles represent the peaks predicted from the asymptotic solution in Eqs. (33) and (35). It is seen that the discrepancy between the maximum load obtained by the two approaches tends to zero for $\bar{\epsilon} \to 0$. For increasing values of $\bar{\epsilon}$ the accuracy of Eq. (35) decreases. However, for an imperfection of 2% the error is only about 4%, which is normally acceptable.

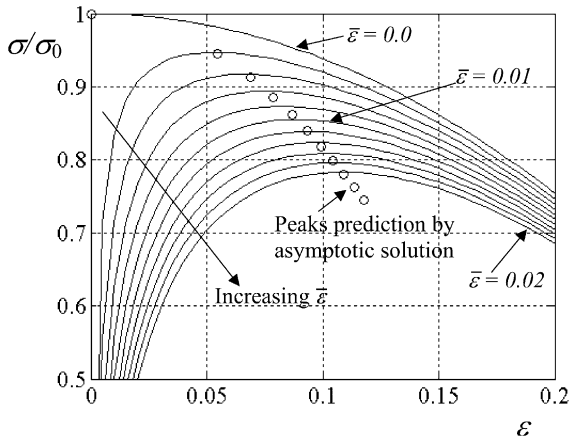

Fig. 7. Reduction in maximum load caused by imperfection sensitivity for $\sigma_2/\sigma_0 = -6.1504$ and various values for the initial imperfection $\bar{\varepsilon}$.

7. Comparison with finite element simulations

Finite element computations corresponding to the case of $L/h = 5$, $E_{ZZ}/E_{XX} = 0.045$, $G_{XZ}/E_{XX} = 0.16$ with $E_{XX} = 5.088$ GPa were carried out using the commercial software package ABAQUS. The homogenized column strip was modelled as a linear elastic orthotropic medium, obeying the constitutive relations given in Eq. (7). CPS8 plane stress elements and a sufficiently fine mesh with 2000 elements were used. One case with a finer mesh of 8000 elements was computed and found to yield no change in the predicted buckling loads. Thus the mesh with 2000 elements was adopted for all the finite element computations. The length of the column was assumed to be 60 mm and the thickness 12 mm (giving an aspect ratio of 5), with a width (in the y-direction) of 1 mm. Clamped–clamped end conditions were assumed. A linear elastic eigenvalue analysis was conducted to obtain the buckling load P_{cr}, giving $P_{cr} = 4600$ N. This value is 4% higher than that predicted by the Engesser formula (see Eq. (4) in Bažant and Beghini, 2005a), which is 4409 N, and 13% lower than the load predicted by the Haringx formula (see Eq. (5) in Bažant and Beghini, 2005a). This confirms once more that a commercial finite element software gives predictions closer to the Engesser formula if the shear modulus is kept constant as discussed in detail in Bažant and Beghini (2004, 2005a,b).

To assess imperfection sensitivity, the initial strip geometry was perturbed by the buckling mode shape, which is shown in Fig. 8. The maximum amplitude of the initial geometric imperfection was set at 1% of the

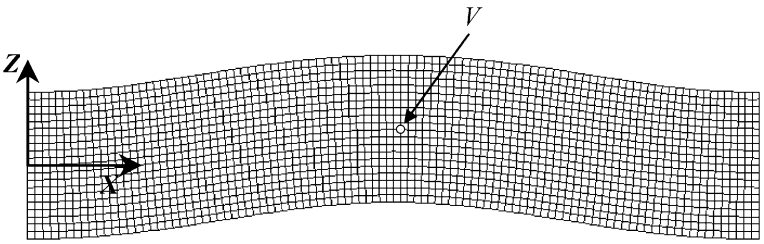

Fig. 8. Buckling mode shape for a clamped–clamped column.

column length L. The right edge of the column was subjected to a known ramp displacement. Because of the possibility of an unstable equilibrium path, the arc length method (Riks, 1972) was used to perform the nonlinear geometric analysis.

Initially, the column response is, as expected, linear (in a plot of P versus the load point displacement or of P versus the deflection of point V in the Z-direction, marked in the buckled mode shape; Fig. 8). With continued loading, as the column approaches the buckling load, the load goes through a maximum, but begins to unload immediately thereafter along an unstable equilibrium path. The maximum load obtained is 94% of the critical load, as indicated in Fig. 9. This may be compared to Koiter's 2/3-power law, Eq. (35), which gives $\sigma_{max}/\sigma_0 = 84\%$ for $\sigma_2/\sigma_0 = -6.1504$.

The finite element prediction for the reduction in maximum load capacity is 10% higher than the prediction of Eq. (35). This is probably due to two main factors. First, the two models are derived from different theories; Eq. (35) stems from a one-dimensional homogenized beam theory approximation, while the elastic finite element analysis is two-dimensional. Second, several approximations have been used to derive Eq. (35); if we compute, for example, the load capacity numerically from Eq. (32) rather than using its asymptotic form Eq. (35), we obtain $\sigma_{max}/\sigma_0 = 85.5\%$. This value is closer to the finite element predictions by 1.5%. Similarly, if we include additional terms in the potential energy (9) or in the expansion (14), we progressively reach the finite element solution. However, the additional analytical burden becomes unbearable and numerical solution becomes the only viable way.

A series of deformed mode shapes corresponding to different points on the response curve (Fig. 10) are shown in Fig. 11 (see Table 2 for location data). Notice that along the unloading path, a secondary instability ('pinching' due to high compression on the lower surface of the column) has occurred at state D, and beyond that state calculations indicate material interpenetration (states E and F), which is impossible. At that stage the finite element results are, of course, unreliable.

To investigate the influence of ratio E_{ZZ}/E_{XX} on the imperfection sensitivity, two other simulations have been carried out for the same aspect ratio $L/h = 5$ with $E_{ZZ}/E_{XX} = 0.2$ and $E_{ZZ}/E_{XX} = 1.0$. As predicted by the analytical results presented earlier, the imperfection sensitivity disappears, as indicated in Fig. 9.

To gain insight into imperfection sensitivity, evolution of the contours of normal stress S_{33} and shear stress S_{13} as a function of load are presented in Figs. 12 and 13 for the case of $L/h = 5$ and $E_{ZZ}/E_{XX} = 0.045$, which is imperfection sensitive, and Figs. 14 and 15 for the case of $L/h = 5$ and $E_{ZZ}/E_{XX} = 1.0$, which is imperfection insensitive (see Table 3 for location of points a, b, c and d). Notice that, in Figs. 12 and 13, the onset of instability (maximum load) coincides with the simultaneous 'stress

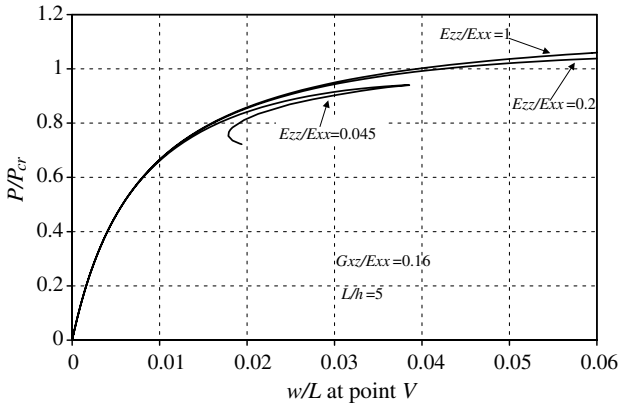

Fig. 9. Load–displacement curves for a short column and three different ratios of E_{ZZ}/E_{XX}.

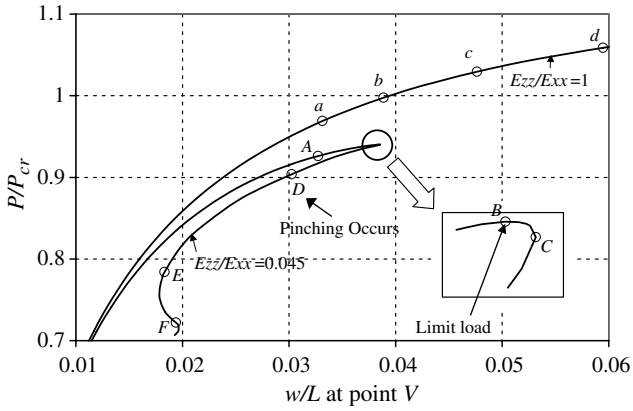

Fig. 10. Detail of two load–displacement curves of Fig. 9. Points A, B are on the loading path, C, D, E, F on the unloading one. Inset shows the peak load. Points a, b, c, d are all on the loading path.

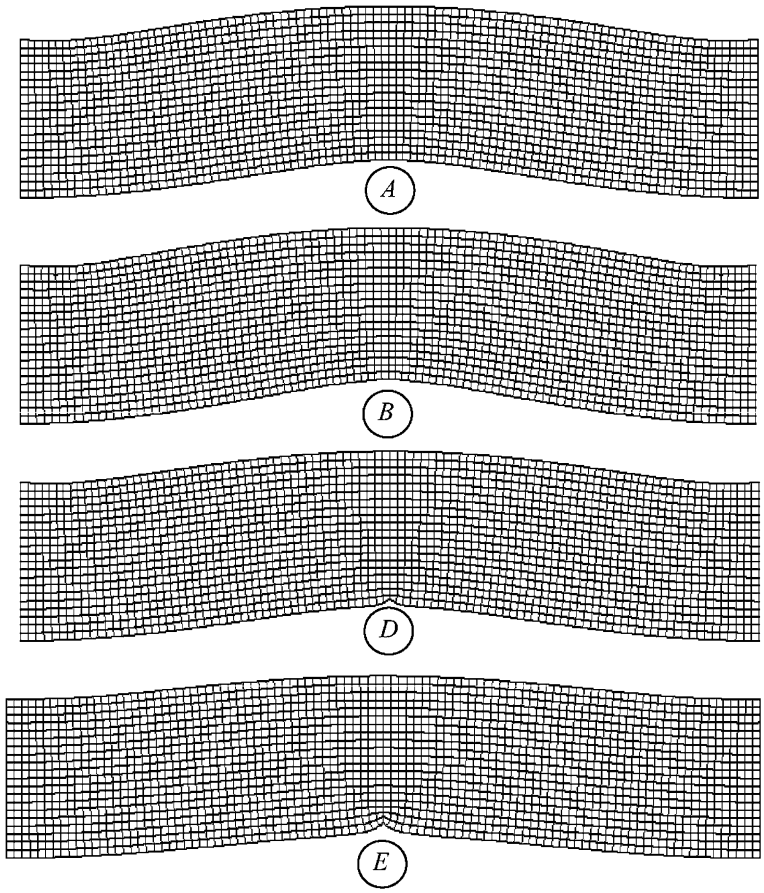

Fig. 11. Deformed shapes of the column with aspect ratio $L/h = 5$, $G_{XZ}/E_{XX} = 0.16$ and $E_{ZZ}/E_{XX} = 0.045$. Location B corresponds to the peak load point.

Table 2
Normalized loads and transverse displacements for which deformed shapes are shown ($E_{ZZ}/E_{XX} = 0.045$)

Location	*A*	*B*	*C*	*D*	*E*	*F*
P/P_{cr}	0.926225	0.940251	0.940170	0.903850	0.784032	0.722105
w/L	0.032739	0.038504	0.038555	0.030245	0.018327	0.019386

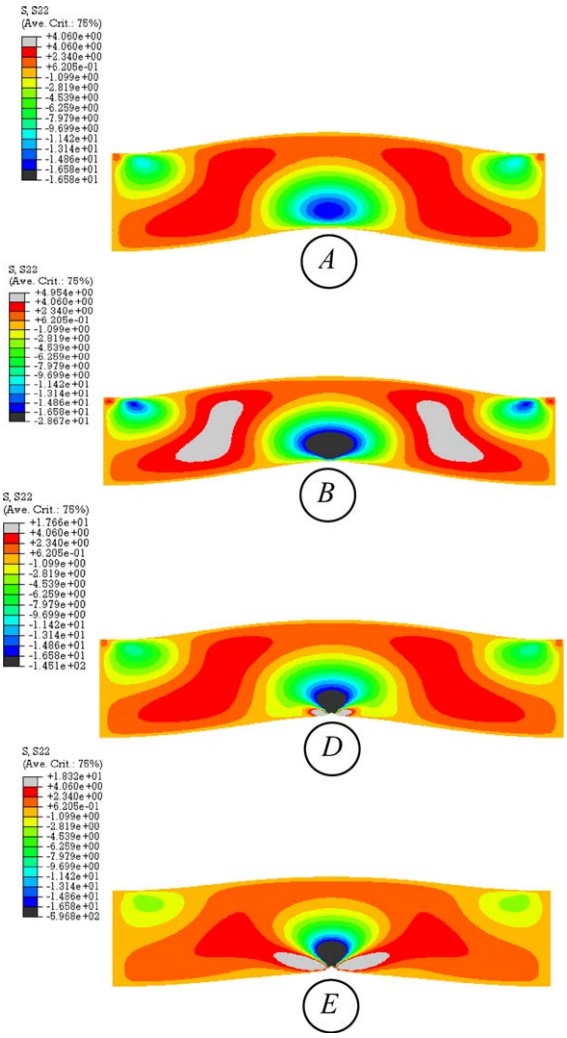

Fig. 12. S_{33} variations for the column analyzed with $E_{ZZ}/E_{XX} = 0.045$.

localization'. Shear and normal stresses, initially more or less uniform, rapidly localize at the bottom surface at mid-length of the column, where, due to the large axial compression, the 'pinching' also causes a large normal component of stress, S_{33}. In contrast, such stress localization and skewing of the stress distribution in the prebuckling regime is not present in the series of contours shown in Figs. 14 and 15. These

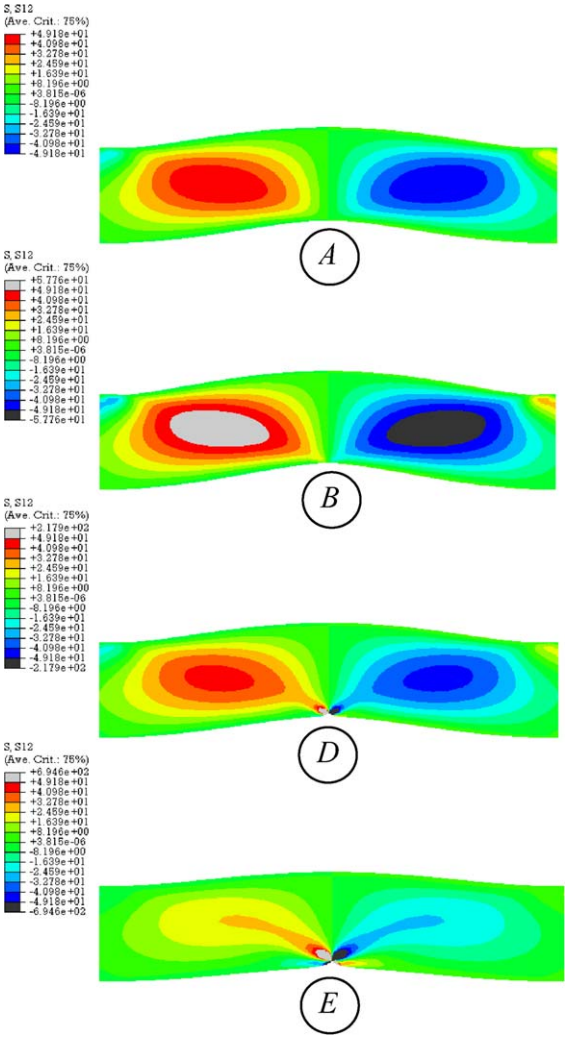

Fig. 13. S_{13} variations for the column analyzed with $E_{ZZ}/E_{XX} = 0.045$.

contour plots clearly show the influence of different material stiffness ratios on the initial postcritical behavior.

8. Explanation of cause of imperfection sensitivity

Experience with finite element analysis suggests a simple, intuitive argument to explain the presence or absence of imperfection sensitivity for the columns analyzed. Consider first the case of $L/h = 5$ and $E_{ZZ}/E_{XX} = 0.045$, as sketched in Fig. 16a and b. In Fig. 16a, half of the column analyzed by finite elements is schematically represented by means of two vertical columns composed of two rigid segments of equal length $L/4$, simulating the external surfaces of the column. The shear stiffness is modelled by rotational springs with stiffness K_{XZ}, while the transverse stiffness is modelled by the two horizontal springs with stiffness K_{ZZ}. The top spring simulates the tensile region around the quarter length, while the bottom one simulates the compres-

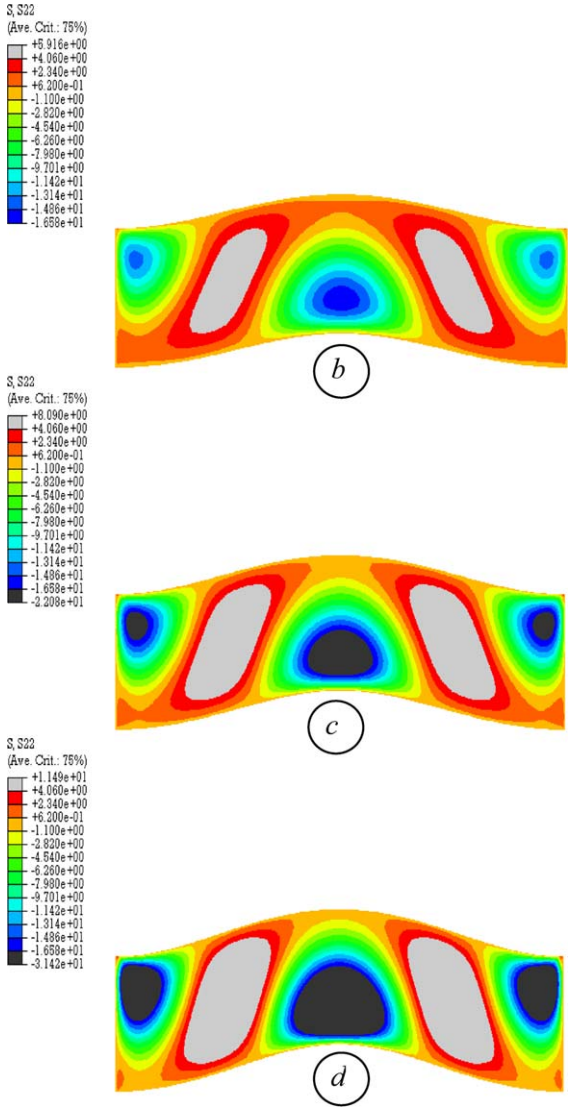

Fig. 14. S_{33} variations for the column analyzed with $E_{ZZ}/E_{XX} = 1$.

sion region around the middle length. The equilibrium equations for the two columns can be written as follows (see Fig. 16b):

$$P_1 L(\sin\theta_1 + \sin\theta_2) - 4K_{XZ}\theta_1 + F_1 L\cos\theta_1 - F_2 L(\cos\theta_1 + \cos\theta_2) = 0 \tag{36}$$

$$P_2 L(\sin\theta_1 + \sin\theta_2) - 4K_{XZ}\theta_2 - F_1 L\cos\theta_2 + F_2 L(\cos\theta_1 + \cos\theta_2) = 0 \tag{37}$$

where P_1 and P_2 are the loads acting on each column; θ_1 is the rotation of the top segment of the left column, which is assumed for simplicity to be equal to the rotation of the bottom segment of the right column; θ_2 is the rotation of the bottom segment of the left column, which is assumed for simplicity to be equal to the rotation of the top segment of the right column; and $|F_1| = |F_2| = K_{ZZ}L(\sin\theta_2 - \sin\theta_1)/4 =$ forces in the springs. The assumption about the rotations implies that the two points of loading, which

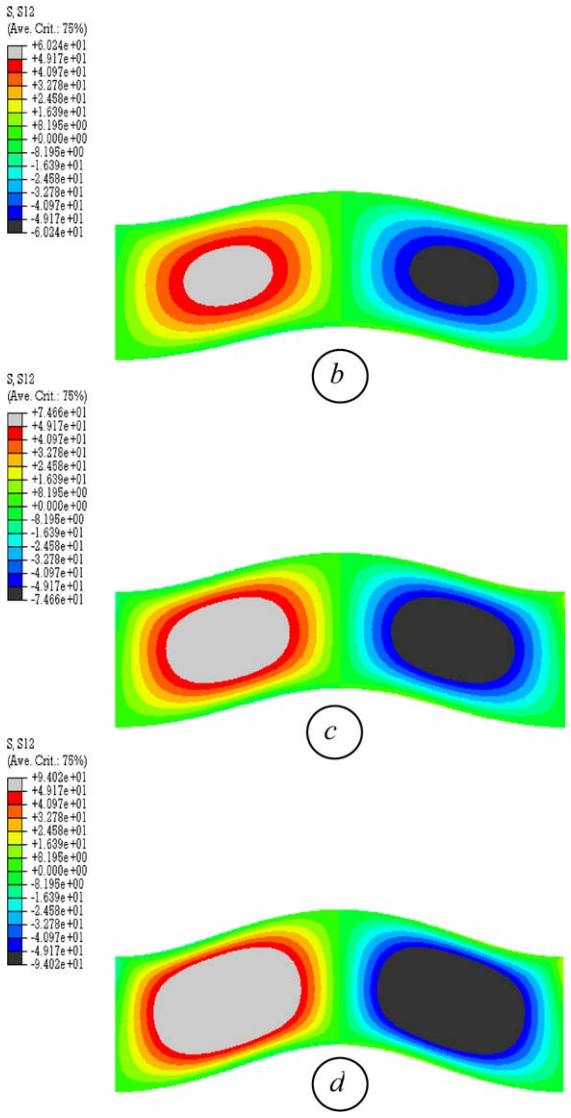

Fig. 15. S_{13} variations for the column analyzed with $E_{ZZ}/E_{XX} = 1$.

Table 3
Normalized loads and transverse displacements for which deformed shapes are shown ($E_{ZZ}/E_{XX} = 1.0$)

Location	*a*	*b*	*c*	*d*
P/P_{cr}	0.969029085	0.997555603	1.029446108	1.058603507
w/L	0.033148833	0.038881500	0.047648833	0.059465833

are sliding vertically downwards, do so together. If we now define the overall load P carried by the system as $P = P_1 + P_2$, we can add the two equilibrium equations (36) and (37), and we obtain:

$$P = 4K_{XZ}\frac{\theta_1 + \theta_2}{L(\sin\theta_1 + \sin\theta_2)} + \frac{K_{ZZ}L}{4}(\sin\theta_2 - \sin\theta_1)\frac{\cos\theta_2 - \cos\theta_1}{\sin\theta_1 + \sin\theta_2} \tag{38}$$

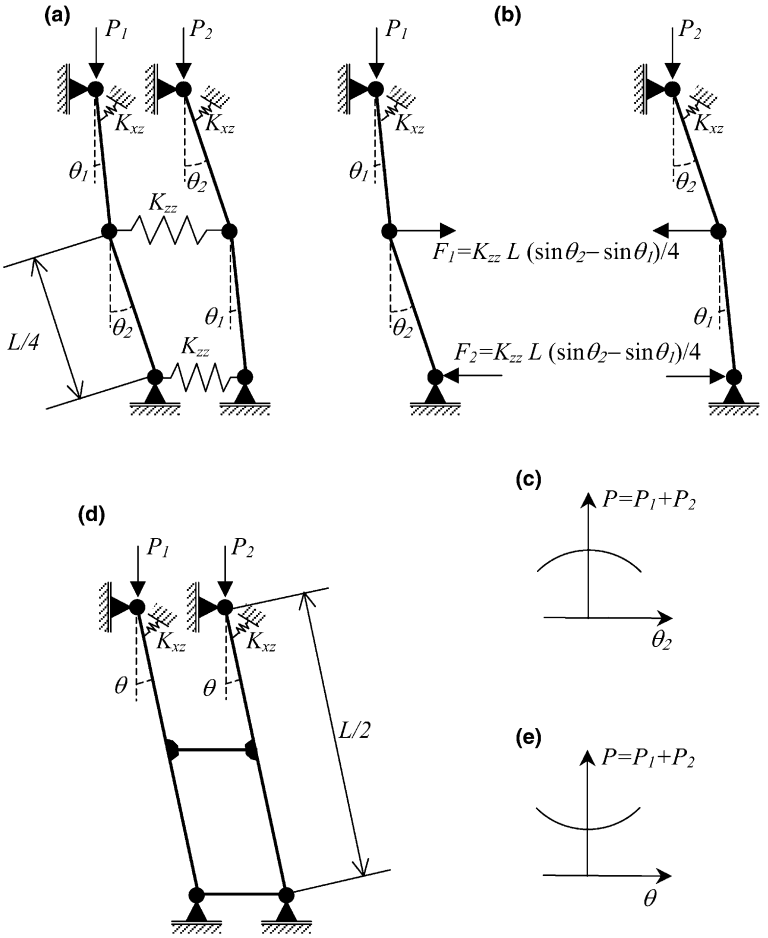

Fig. 16. (a) Schematic representation of the column with $E_{ZZ}/E_{XX} = 0.045$; (b) forces acting in the system; (c) imperfection sensitive behavior for the column with $E_{ZZ}/E_{XX} = 0.045$; (d) schematic representation of the column with $E_{ZZ}/E_{XX} = 1.0$, and (e) its imperfection insensitive behavior.

If we introduce here the Taylor series expansion for the sine and cosine functions and assume that $\theta_2 \gg \theta_1$, we obtain, with second-order accuracy:

$$P = \frac{4K_{XZ}}{L} + \theta_2^2\left(\frac{2K_{XZ}}{3L} - \frac{K_{ZZ}L}{8}\right) \tag{39}$$

This expression implies imperfection sensitivity of the structure, as sketched in Fig. 16c, for the stiffness values satisfying the inequality:

$$\frac{K_{XZ}}{K_{ZZ}L^2} < \frac{3}{16} \tag{40}$$

This explains in a more intuitive manner than the rigorous and complex variational analysis why there is imperfection sensitivity for the column with $L/h = 5$ and $E_{ZZ}/E_{XX} = 0.045$.

An alternative point of view is to observe (Fig. 16a) that the lateral deflections of the two columns interact during buckling. As shown in detail by Koiter (1945) and also explained by Bažant and Cedolin (1991, Section 4.6), interaction of modes usually causes imperfection sensitivity, as it does in this case.

On the contrary, if we consider the case $L/h = 5$ and $E_{ZZ}/E_{XX} = 1$, the column can be sketched as in Fig. 16d. The external surfaces of the column are now represented as a single rigid bar and the horizontal springs are replaced by rigid connections. In this case the rotations of the two columns are the same: $\theta_1 = \theta_2 = \theta$. Therefore, the load carrying capability of the system can simply be derived as a particular case of Eq. (38):

$$P = 4K_{XZ}\frac{\theta}{L\sin\theta} = \frac{4K_{XZ}}{L}\left(1 + \frac{\theta^2}{6}\right) \tag{41}$$

This expression implies that the structure exhibits no imperfection sensitivity, as sketched in Fig. 16e, and agrees with what the finite element analysis shows.

These simple examples show in an intuitive manner that imperfection sensitivity stems from the localization of stresses into the core with a low transverse stiffness. This is confirmed by the fact that similar studies (e.g., Huang and Kardomateas, 2000) conducted on sandwich beams including the shear deformability of the structure but neglecting the transverse deformability show no imperfection sensitivity.

9. Remarks on internal instability and mode interaction

The analytical model described in the previous sections captures the instability due to buckling, which is the most important instability mode that may be encountered in practice for highly orthotropic structures. However, there are some instabilities which cannot be accounted for by applying the kinematic model (3) with the constitutive model (7) for sandwich structures and, in general, for structures reinforced in the direction of the applied load. In particular, the present formulation cannot describe the wrinkling of the

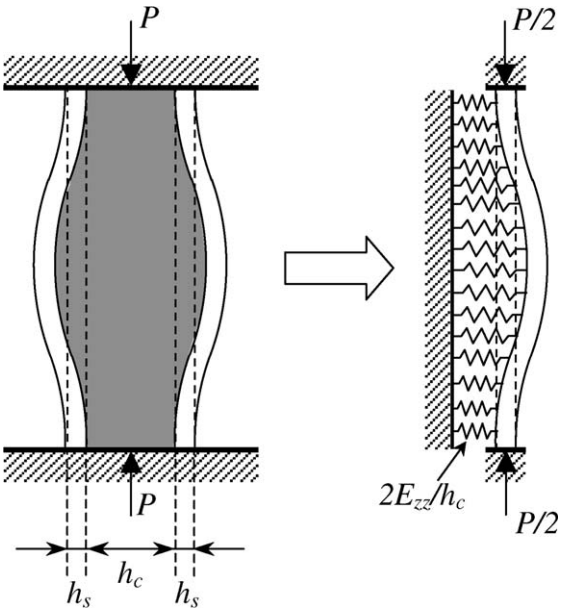

Fig. 17. Bulging instability for a sandwich column (left) and its interpretation (right).

skin or the bulging of sandwich columns, which are cases of surface and internal instabilities (Bažant and Cedolin, 1991, Sec. 11.7).

The bulging instability is depicted in Fig. 17 for the case of a sandwich column with skin thickness h_s and core thickness h_c such that $2h_s + h_c = h$. If the wavelength is not shorter than the core thickness h_c, this instability can be schematically analyzed by assuming that the skins are acting as beams on an elastic foundation (Bažant and Cedolin, 1991) carrying one half of the overall load P on the sandwich (see Fig. 17 on the right). The stiffness c of the springs per unit length of column is $c = 2E_{ZZ}/h_c$, and from this the critical load for the skin instability is obtained as

$$P_{cr} = 4\sqrt{cE_s h_s^3/12} \tag{42}$$

where E_s is the longitudinal modulus of the skin, which is assumed to be approximatively equal to E_{XX}.

The bulging instability interacts with the global buckling described in the previous sections if the Engesser critical load, given by Eq. (23), is close to the bulging load, given by Eq. (42). To understand if this may happen in practical applications, let us consider the column analyzed by finite element with $E_{ZZ}/E_{XX} = 0.045$ and $L/h = 5$. In this case, the two critical loads would be equal for skin thickness $h_s = 0.5$ mm, which corresponds to the ratio $h_s/h_c = 1/20$. In most practical applications $h_s/h_c \geqslant 1/10$, in particular for $h_s/h_c = 1/10$ the bulging critical load of the sandwich column considered is twice the Engesser load. Therefore, the instability would be of the type described in the previous sections, without interaction with the bulging. Note, however, that if a sandwich with $h_s/h_c = 1/20$ is used, the interaction occurs and a detailed investigation by finite elements is then required to assess the effect of this interaction.

Other types of instability, described in detail in Bažant and Cedolin (1991) (Sec. 11.7), are characterized by a critical load significantly higher than the Engesser load; therefore, they are not involved in common applications.

In conclusion, for most practical situations the interaction of different instability modes can be neglected because the buckling instability dominates.

10. Conclusions

1. The general method for initial postcritical analysis of structures with low shear and *transverse stiffness* presented in this study is a useful tool to verify the numerical solutions obtained, e.g., by finite elements.
2. For linearly deforming clamped–clamped short columns deforming linearly with Doyle–Ericksen tensors of parameter $m = 2$ or $m = 1$, there is a stiffness range for which the structure exhibits imperfection sensitivity. The maximum load of such columns is reduced, and the collapse is dynamic if the load is controlled.
3. Comparison with finite element analysis of short columns shows that the present analytical formulas predict the maximum load quite accurately.
4. Imperfection sensitivity of sandwich columns can be caused by transverse deformations of the core. If these are neglected, imperfection sensitivity can be missed.
5. Sandwich columns and, more generally, columns reinforced in the direction of the applied load may exhibit interaction of instability modes, particularly buckling and bulging. However, the buckling instability dominates in most cases.

Acknowledgements

Financial support under Grant N00014-02-I-0622 from the Office of Naval Research to Northwestern University (monitored by Dr. Yapa D.S. Rajapakse) is gratefully acknowledged.

References

Bažant, Z.P., 1971. A correlation study of incremental deformations and stability of continuous bodies. J. Appl. Mech., ASME 38, 919–928.

Bažant, Z.P., 2003. Shear buckling of sandwich, fiber-composite and lattice columns, bearings and helical springs: paradox resolved. J. Appl. Mech., ASME 70, 75–83.

Bažant, Z.P., Beghini, A., 2004. Sandwich buckling formulas and applicability of standard computational algorithm for finite strain. Composites: Part B 35 (6–8), 573–581.

Bažant, Z.P., Beghini, A., 2005a. Which formulation allows using a constant shear modulus for small-strain buckling of soft-core sandwich structures? J. Appl. Mech., ASME 72 (5), 785–787.

Bažant, Z.P., Beghini, A., 2005b. Stability and finite strain of homogenized structures soft in shear: sandwich or fiber composites, and layered bodies. Int. J. Solids Struct., in press, doi:10.1016/j.ijsolstr.2005.03.060.

Bažant, Z.P., Cedolin, L., 1991. Stability of Structures: Elastic, Inelastic, Fracture and Damage Theories. Oxford University Press, New York, and republication with updates, Dover Publ., New York, 2003.

Huang, H., Kardomateas, G.A., 2000. Buckling and initial postbuckling behavior of sandwich beams including transverse shear. AIAA J. 40 (11), 2331–2335.

Koiter, W.T., 1945. Over de Stabiliteit van het Elastische Evenwicht. Dissertation, Delft, Holland, Translation: On the Stability of Elastic Equilibrium. NASA TT-F-10833, 1967 and AFFDL-TR-70-25, 1970.

Novozhilov, V.V., 1953. Nonlinear Elasticity. Graylock Press, New York.

Riks, E., 1972. The application of Newton's method to the problem of elastic stability. Trans. ASME, J. Appl. Mech. 39 (4), 1060–1065.

Stein, M., 1985. Postbuckling of long orthotropic plates in combined shear and compression. AIAA J. 23, 788–794.

Stein, M., 1989. Effects of transverse shearing flexibility on postbuckling of plates in shear. AIAA J. 27, 652–655.

Stein, M., Jegley, D., 1987. Effects of transverse shearing on cylindrical bending, vibration and buckling of laminated plates. AIAA J. 25, 123–129.

Stoker, J.J., 1968. Nonlinear Elasticity. Gordon and Breach, New York.

Waas, A.M., 1990. Initial postbuckling behavior of beams on non-linear elastic foundation. Mech. Res. Commun. 17 (4), 239–248.

Waas, A.M., 1992. Initial postbuckling of shear deformable symmetrically laminated beams. Int. J. Non-linear Mech. 27 (5), 817–832.